Curli-producing *E. coli* enhances the disease phenotype in an hSOD1 G93A mouse model of ALS

Zimple Kurlawala (zimple.kurlawala@louisville.edu)
University of Louisville https://orcid.org/0000-0003-3925-9290

Article

Keywords: E. coli, ALS, microbiome, curli

Posted Date: September 1st, 2021

DOI: https://doi.org/10.21203/rs.3.rs-506373/v1

Abstract

Amyotrophic Lateral Sclerosis (ALS) is a rapid and fatal neuromuscular degenerative disease which has no known genetic cause in ~ 90% of cases. We explored the microbiome as a potential non-genetic contributing factor for the disease. Microbial dysbiosis in the gut can occur due to diet, lifestyle and environmental factors and differences in gut microbial communities have been detected between ALS subjects and healthy controls, including an increase in *E. coli* in ALS subjects. *E. coli* and other physiological gram-negative bacteria produce curli proteins which are functional bacterial amyloid fibrils. Curli fibrils form biomatrices and interact with several proteins in the extracellular matrix, such as CD14, Toll-like receptors and MHC1 molecules expressed on the surfaces of all nucleated cells. Over-exposure to curli in the gut enhanced neuroinflammation and alpha synuclein misfolding in the brain in a rodent model of Parkinson's disease. In this study, we examined whether curli exposure can exacerbate the development and progression of ALS. We utilized the hSOD1 G93A mouse model of slow developing ALS, with their inherent microbiome on a normal chow diet. These mice were fed curli-producing or curli-nonproducing (mutant) *E. coli* in applesauce 3 times/week from 4 weeks of age to 6 months. Chronic consumption of *E. coli* was well-tolerated by all mice, measured regularly by signatures of general wellness. Male hSOD1 mice demonstrated faster ALS progression compared to female hSOD1 mice. Chronic exposure to *E. coli* significantly shifted bacterial and viral alpha and beta diversities in the gut of all mice. Curli-fed mice showed significant decrease in relative abundance of *Proteobacteria* phyla. Within the male hSOD1 cohort, curli-fed mice exhibited locomotive signs of faster ALS progression, increased markers of skeletal muscle atrophy, increased inflammation in the muscle and spinal cord, and suppressed peripheral immune responses compared to mutant-fed and vehicle mice. Within the female cohort, exposure to both curli-producing and mutant *E. coli* suppressed peripheral immune responses. In conclusion, over-exposure to curli-producing *E. coli* in the gut worsened the pathological, immunological and motor features of ALS, in the absence of overt signs of illness. These results suggest that opportunities for manipulation of the gut microbiome in ALS need to be explored.

Introduction

Amyotrophic lateral sclerosis (ALS) is a rapidly progressive, fatal neuromuscular degenerative disease, with symptoms developing between the ages of 40–70 years. Current treatments modestly slow the progression of the disease but there is no known cure. ALS is familial in only ~ 10% of cases, and can affect anyone worldwide regardless of racial, ethnic, or socioeconomic status. In majority of the cases the initiating factor responsible for the illness is not known. The heterogeneity of possible risk factors[1] such as intense exertion, toxins, metals, chemicals, and trauma, electromagnetic field exposure, military service point to the involvement of environmental factors in the etiology of ALS.

The human microbiome is a potential environmental risk factor for ALS. The microbes inhabiting our body are our largest environmental influence and their effect on neurodegenerative disorders is just now being explored. The presence of an unhealthy population of microbes in the body is referred to as dysbiosis. Microbial dysbiosis in the gut can occur due to diet, lifestyle and environmental factors and

may present in several different ways. Small intestine bacterial overgrowth, one form of dysbiosis, is often found in older adults and can manifest with diarrhea, malabsorption, nutritional deficiencies, osteoporosis, and weight loss[2]. Most of the time, bacterial overgrowth does not cause overt symptoms but may contribute to chronic pathologies such as cancer[3–5].

Recent work has suggested an association of abnormal gut microbial communities and ALS. Clinical studies revealed that there are differences in microbial populations between ALS subjects and healthy controls. Di Gioia et al found a significant increase in the gut *E. coli* population in ALS patients[6]. These phenomena have been recapitulated in experimental models of mice harboring human ALS mutations. Supplementing probiotic bacteria[7] and the bacterially produced metabolite butyrate[8], increased lifespan in a hSOD1 G93A model of ALS. We have shown that gut exposure to a functional bacterial amyloid (FUBA) protein called curli, enhances inflammation and amyloid misfolding in the brain in a rodent model of Parkinson's disease. These studies have received support from work of Sampson et al in Parkinson model transgenic mice[9]. Curli protein fibrils are normally produced by *E. coli* and other gram-negative bacteria which contribute to bacterial biomatrices (biofilms) and enhance adhesion to surfaces. Curli fibrils interact with several proteins in the extracellular matrix, such as CD14[10], Toll-like receptors[11, 12] and MHC1[13] molecules-expressed on the surfaces of all nucleated cells. Notably, the ability of curli fibers to initiate misfolding of neuronal proteins such as amyloid beta and alpha synuclein have been demonstrated[14–16].

ALS is known to have a variable location of symptom onset with some patients having trouble with swallowing or speech at an early stage, while others may have onset with weakness in the lower extremities. These variable modes of presentation certainly relate to location of onset of anterior horn cell dysfunction. It has been proposed that the factors responsible for this variable presentation is the location at which the microbiota are interacting with the central nervous system (88).

In this study, we examined whether curli exposure exacerbates the development and progression of ALS. We utilized the hSOD1 G93A mouse model of ALS and exposed them to curli producing *E. coli* and control (*E. coli* lacking curli) bacteria for 6 months. Mice were regularly assessed for measures of general wellness, disease progression and immune function. Within the male hSOD1 cohort, curli-fed mice showed locomotive signs of faster ALS progression, increased markers of skeletal muscle atrophy, increased inflammation in muscle and spinal cord, and suppressed peripheral immune responses compared to mutant-fed and vehicle mice.

Results

Study Design

We utilized the hSOD1 G93A mouse model of familial ALS on a C57/Bl6 background[17]. This hSOD1-G93A strain exhibits a slower ALS motor phenotype at six to seven months of age as it has a reduced

copy number of the transgene, compared to the original strain. We analyzed a total of 91 animals (Fig. 1A). To assess the role of curli exposure and dysbiosis, we introduced *E.coli* via food as previously described[18]. Overall, three groups were assessed: 1) vehicle only (no bacteria added); 2) mutant *E. coli* (lacking the CsgA operon, E. coli K-12 BW25113), and 3) wild-type *E. coli* (BW25113[19] bearing the CsgA operon, involved in the production of curli), referred to as *E. coli* curli in this manuscript. Bacteria were fed to mice 3 times a week for 6 months (Fig. 1B). PCR data (Fig. 1C) and bacterial cultures (Fig. 1D) from fecal pellets collected on a non-feeding day confirmed the over-expression of CsgA gene in the curli group and genotype and sex of the animals did not alter CsgA expression. The hSOD1 G93A gene copy number was not different between bacterial feeding groups (Fig. 1E) or sex of mice (Supp. Figure 1A). We analyzed data for males and females separately as it is well established that the rate of ALS development in females is slower than males[20]. There were no significant effects of genotype or bacterial feeding on body weights of mice from 1–7 months of age (Fig. 1E,F).

Bacterial feeding caused significant shifts in alpha and beta diversity of gut bacteria and viruses

Fecal pellets collected from mice at 6 months of age were submitted for whole-genome shallow shotgun sequencing. Reliable hits were obtained for bacteria and viruses utilizing the CosmosID metagenomics platform. We assessed effects of the three feeding groups on microbial diversity, composition, and taxonomic alterations. Diversity within individual samples was evaluated using the alpha diversity measure - Shannon Index (measuring species abundance and evenness). Within the male hSOD1 groups, bacterial diversity was reduced in the curli group (Fig. 2B) as compared to both vehicle ($p < 0.05$) and mutant (trending, $p = 0.08$) groups, whereas viral diversity was significantly reduced in the curli group (Fig. 2F) as compared to the mutant group ($p < 0.05$). Compositional changes between the samples were evaluated by the beta diversity measure, JACCARD index (similarity distance matrix). For bacterial species, male hSOD1 cohort showed significant clustering of the curli fed animals (Fig. 2J), $p = 0.001$ calculated by PERMANOVA analyses. For viruses, male hSOD1, female WT, and female hSOD1 cohorts showed significant clustering of both bacterial-fed groups compared to vehicle (Fig. 2N-P), $p < 0.01$ calculated by PERMANOVA analyses.

Alterations in taxonomy were assessed by comparing quantitative data (relative abundance) between groups. Interestingly, in all cohorts, the relative abundance of phylum *Proteobacteria* was significantly reduced by exposure to curli producing *E. coli* (Fig. 2Q-T). At the level of viral phylogeny, hSOD1 mice showed significant expansion of gammaretrovirus genera compared to WT animals, but only for males (Supp. Figure 1B, C). Depletion and enhancement of several bacterial and viral strains were observed in response to mouse genotype, sex, and bacterial feeding, and a detailed list is provided in supplementary data (Supp. Figure 1D, E).

Overall, these results indicate that, i) alpha diversity is perturbed by curli feeding in the male hSOD1 cohorts, ii) microbial composition is distinct between the feeding groups, and iii) observed changes in the bacterial microbiome may be primarily attributed to shifting in the relative abundance of phylum *Proteobacteria.*

Chronic gut exposure to mutant and curli-producing E. coli accelerated skeletal muscle atrophy and TLR2 expression in hSOD1 male mice

SOD1-positive aggregations in skeletal muscles are a hallmark of familial cases of ALS and we detected these in the tibialis anterior muscle utilizing an antibody specific for hSOD1 G93A protein (MS785, GTX57211). Within the male hSOD1 cohort, both mutant and curli-fed mice showed increased SOD1-positive staining compared to vehicle (Fig. 3A, B). Additionally, we examined gastrocnemius, tibialis anterior and quadriceps skeletal muscle tissues for several markers of muscle atrophy. Within the male hSOD1 cohort, p62 and Beclin1, markers of autophagy, were significantly increased in both bacterial groups (Fig. 3C). TNFa, a well-known muscle cachectin, was significantly increased in skeletal muscles of both mutant and curli producing *E. coli* cohorts (Fig. 3D). Arginase 1 and CD38 (trending), markers of activated macrophages (Fig. 3E); and MurF1, an E3 ubiquitin ligase, were significantly upregulated only in the curli fed group (Fig. 3F) indicating increased tissue inflammation and muscle turnover in this cohort. Transcription of TLR2, a pathogen recognition receptor was increased 1.4-fold in the muscle in the curli fed group (Fig. 3G). Concurrent with increased markers of muscle atrophy, curli fed male hSOD1 mice had significantly lower weights of the quadriceps muscle (Fig. 3H) compared to vehicle ($p = 0.007$).

Overall, in the male hSOD1 cohort, chronic feeding of both mutant and curli producing *E. coli* increased several markers of atrophy in distal skeletal muscles, and these were significantly worse in curli-fed groups compared to mutant-fed groups. Curli fed mice also had more TLR2 expression and more muscle atrophy.

SOD1 males exposed to curli-producing E. coli demonstrated earlier locomotive abnormalities as measured with BMS and TreadScan

Starting at 3 weeks of age up to 7 months, we measured open-field locomotor characteristics of hind limbs by Basso Mouse Scale (BMS)[21] and gait kinematics utilizing a well-established highly sensitive tool called TreadScan[22]. Both, male and female hSOD1 mice demonstrated a decrease in BMS scores as ALS developed (Fig. 4A-D). However, the decline in male hSOD1 mice started earlier, around 4 months of age (Fig. 4B) whereas female hSOD1 BMS scores declined month 5 onwards (Fig. 4D). Within the male hSOD1 cohort, curli fed mice demonstrated a trend towards decreased BMS scores compared to vehicle and mutant fed mice at month 6 ($p = 0.1$) (Fig. 4B). Gait characteristics measured with TreadScan every month assessed gradual development of locomotor abnormalities in mice. Compared to male WT mice, around 6 months of age, male hSOD1 mice demonstrated slowing in running speed ($p = 0.019$, Supp Fig. 2A) and decrease in hind limb stride time ($p = 0.02$, Supp. Figure 2B). Within the male hSOD1 cohort, curli fed mice showed shortening in stride length at month 6 (Fig. 4I), maximum lateral deviation of hind feet from the axis of the body (Fig. 4J), inability to efficiently move the body from a straight axis (Fig. 4K) and a smaller paw print area of the hind feet (Fig. 4L). No significant locomotive abnormalities were detected in female hSOD1 mice by TreadScan analyses.

Overall, curli fed hSOD1 males showed significant locomotive anomalies compared to vehicle and mutant fed hSOD1 males measured with BMS and Treadscan analyses.

Chronic gut exposure to mutant and curli-producing E. coli increased astrocytosis in the brain and demyelination in the spinal cord

As expected in this lower motor neuron degenerative disease, cholinergic neurons detected by choline acetyltransferase (ChAT) immunostaining were significantly decreased in the spinal cord in hSOD1 mice compared to WT (Fig. 5A, B). Interestingly, WT mice with bacterial exposure to mutant and curli producing *E. coli* showed significant reduction in ChAT positive neurons compared to vehicle (Fig. 5B). Non-neuronal cells such as astrocytes and microglia can exacerbate ALS progression in addition to the primary damage caused by mutated hSOD1 in neuronal and muscular cells[23]. hSOD1 mice showed increased astrocytosis (GFAP, Fig. 5C) and microgliosis (Iba1, Fig. 5D) in the lumbar spinal cord compared to WT animals, but within the hSOD1 cohort, bacterial feeding did not significantly alter these markers. However, the brainstems of curli-fed mice were highly astrocytic (GFAP) compared to mutant and vehicle groups ($p = 0.03$) (Fig. 5E,F) but there were no significant differences in microgliosis (Iba1 immunostaining, data not shown). Mice exposed to both bacterial groups showed significantly more demyelinated white matter in the spinal cord as compared to the vehicle group ($p = 0.006$), measured with Luxol Fast Blue stain (Fig. 5G, H).

Overall, chronic feeding of mutant and curli producing *E. coli* in the gut decreased cholinergic neurons and myelination in the spinal cord. Chronic feeding of curli producing E. coli increased astrocytosis in the brainstem compared to mutant and vehicle fed groups.

Chronic gut exposure to E. coli did not increase gut permeability

We measured gut barrier function in distal colon of live mice with oral administration of FITC-Dextran at 6 months and ZO-1 mRNA expression post-mortem. We found no indication of a gut barrier breach, regardless of genotype and bacterial feeding (Fig. 6A,B; Females-Supp. Figure 3A). There were no significant changes in gastric motility at 6 months measured as time taken (hours) for the appearance of a red pellet after with oral administration of carmine red dye (Fig. 6C). Several markers of inflammation were probed for in the distal colon by qRT-PCR (Fig. 6D and females, Supp. Figure 4B-C)) and Western Blot analyses (data not shown). IL22, produced by activated T cells and play a role in potentiating pro-inflammatory responses[24] were slightly decreased (trending) in curli-exposed male hSOD1 mice (0.9-fold vs. vehicle) (Fig. 6D). No other cytokines in the colon were significantly different between the bacterial feeding groups. Routine morphological examination of the distal colon by H&E staining did not show significant differences between number or type of mucosal and laminar immune cell aggregations between genotype, sex or bacterial feeding groups (data not shown).

Overall, there were no indications of increased gut permeability in hSOD1 G93A mice or in any bacterially fed groups measured by FITC-Dextran absorption in peripheral blood. Curli-exposed male hSOD1 mice showed slightly decreased IL22 mRNA expression vs. mutant-fed group in distal colon.

Chronic gut exposure to curli-producing E. coli in the gut suppressed peripheral immune responses in hSOD1 male mice

Starting at 3 weeks of age, up to 7 months, we examined changes in circulating immune cell populations and cytokines in peripheral blood. The most striking finding was the significant increase of B cells ($CD3^-$ $CD19^+$) in male hSOD1 mice compared to male WT mice, month 3 onwards (Fig. 7A). Female hSOD1 mice did not demonstrate this increase (Fig. 7B). Bacterial feeding did not influence peripheral B cell population (Fig. 7C, Supp. Figure 4A, B). In the male hSOD1 cohort, curli-fed mice showed significantly decreased expression of several innate immunity markers such as NK cells ($CD3^-$ NK1.1, Fig. 7D), plasmacytoid dendritic cells ($CD3^-$ $CD11b^-$ $CD11c^+$, Fig. 7E), and monocytes ($CD3^-$ $CD11b^-$ $Ly6c^+$, Fig. 7F). In the adaptive immune arm, curli exposed animals had significantly decreased expression of $CD4^+$ T_H cells (Fig. 7G) and $CD4^+CD25^+$ activated T_H cells (Fig. 6H). There were no significant differences in cytotoxic T_C cell expression ($CD8^+$ T cells, Fig. 7I) but activated $CD8^+$ $CD25^+$ T_C cells were significantly decreased in curli exposed males. Additionally, expression of peripheral blood cytokines, CXCL10 (Fig. 7K) at 3 months and eotaxin (Fig. 7L, trending $p = 0.06$) at 6 months, which play a crucial role in recruitment of T cells into sites of tissue inflammation[25–28] were also decreased in curli-fed hSOD1 males. In females, both mutant and curli producing *E. coli* groups showed significant suppression of the above innate and adaptive immune markers. (Supp. Figure 4B-K)

Overall, chronic feeding of curli producing *E. coli* led to suppressed peripheral immune responses in males, whereas both mutant and curli producing *E. coli* led to suppressed peripheral immune responses in females.

Discussion

We examined the role of *E. coli* induced dysbiosis in progression of ALS and found that curli producing *E. coli*, but not *E. coli* mutant (lacking genes for curli production), exacerbated ALS in male hSOD1 G93A mice. Male mice chronically exposed to *E. coli* curli in the gut demonstrated significantly decreased abundance of the Proteobacteria phylum, decreased microbial species diversity, unique clustering of beta diversity, and significant abnormalities in locomotive function indices that developed earlier than in the vehicle and *E. coli* mutant groups. Additionally, curli exposed hSOD1 males experienced accelerated skeletal muscle atrophy, higher transcriptional expression of TLR2, Beclin1, p62 and MurF1, increased SOD1 immunostaining in skeletal muscle, increased expression of macrophage markers arginase 1 and CD38, and increased protein expression of TNFa, all well-established markers of muscle atrophy in ALS. Curli exposed animals also demonstrated increased astrocytosis in the brainstem.

Intestinal dysbiosis is commonly associated with gastrointestinal diseases and there is increasing evidence that microbiome composition may influence development of neurodegenerative disorders such as Parkinson's disease[9, 18, 29], ALS[7, 30–32] and Alzheimer's disease[33, 34] as well as autism spectrum disorder[35, 36], and depression[37]. Recently, it was reported that there is significant expansion of the *E. coli*

population in the gut of ALS patients compared to healthy controls[30]. Bacterial overgrowth in the intestine is found in approximately 20% of healthy older adults, manifested by mild symptoms such as malabsorption[2] but dysbiosis can be clinically silent in the majority of cases. The role of chronic dysbiosis has not been extensively studied in ALS.

We produced chronic dysbiosis in a mouse model of ALS that had a standard microbiome for its strain and housing facility. Exogenous introduction of a commensal bacteria such as curli-producing *E. coli* shifted the gut microbial composition to induce bacterial and viral dysbiosis in these mice. *E. coli* usually inhabit the small intestine and belong to the gammaproteobacterial class of the phylum *Proteobacteria* and are typically associated with inflammatory conditions such as obesity[38] and inflammatory bowel disease[39]. Treatment with *E. coli*-curli significantly inhibited proliferation of *Proteobacterial* species in the distal colon. Curli fibrils interact with several proteins in the extracellular matrix, such as CD14[10], Toll-like receptors[11, 12] and MHC1[13] molecules - expressed on surfaces of all nucleated cells. We found that curli-exposed hSOD1 male mice have higher expression of TLR2 in skeletal muscle compared to those exposed to mutant bacteria. This finding confirmed our earlier demonstration of a similar TLR2 response in aged rats exposed to curli[18, 40, 41]. Since curli proteins exhibit high affinity for MHC1 and their interaction enhances adhesion and colonization of bacteria, such an interaction can potentially interfere with the antigen presenting function of MHC1 molecules to cytotoxic T cells[13]. This phenomenon may be responsible for an overall suppressed peripheral immune response in mice chronically fed with *E. coli*-curli. At 7 months of age, expression of T_H cells ($CD4^+$), activated T_H cells ($CD4^+CD25^+$), NK cells ($CD3^-$ NK1.1), dendritic cells ($CD11b^-$ $CD11c^+$) and monocytes ($CD11b^+$ $Ly6c^+$) were significantly decreased in the peripheral blood of curli exposed males. T cell chemoattractant cytokines such as CXCL10 and eotaxin in peripheral blood and IL22 in the colon were also decreased. Several published reports of ALS patients revealed that expression of $CD4^+CD25^+$ T cells correlate inversely with rapid ALS progression[42–44], similar to our findings in curli-exposed hSOD1 males. While curli exposed mice had a dampened peripheral immune response, inflammation at the tissue level was enhanced as evidenced by greater infiltration of macrophages (Arginase 1 and CD38) and increased TNFa expression in skeletal muscles. The role of peripheral inflammation in ALS is poorly understood, with conflicting reports of whether peripheral inflammation is beneficial or harmful to the disease process[45]. Our data raise the possibility that suppression of the peripheral immune response accelerated skeletal muscle atrophy in curli-exposed hSOD1 male mice, also famously postulated by the Appel research group[42, 44, 46].

We examined the skeletal muscles of mice for several markers of inflammation and atrophy. Mice exposed to bacteria (both, *E. coli*-curli and mutant) exhibited increased hSOD1 immunostaining and TNFa protein expression, suggesting activation of pro-inflammatory pathways in skeletal muscles. Concurrently, curli-exposed mice displayed significantly higher expression of Beclin, p62 (autophagy markers) and Murf1 (E3 ligase) mRNA and significantly lower weights of the quadriceps muscle, collectively indicating muscle atrophy. It is well-established that in both familial and sporadic ALS subjects, skeletal muscles harbor impairment in protein quality control processes such as autophagy[47, 48

and proteasomal degradation[49–53]. Autophagy is upregulated in ALS secondary to accumulation of insoluble protein aggregates, stress granules, and damaged mitochondria. Expression of E3 ubiquitin ligases such as Murf1, Mafbx (Atrogin1) and Musa1 positively correlate with muscle atrophy as these ligases target proteins for degradation during muscle atrophy and remodeling[49, 53]. A skeletal muscle only knock-in model of the hSOD1 G93A transgene could develop an ALS phenotype in mice[54], suggesting that skeletal muscle develops its own pathology independent of lower motor neuron (LMN) degeneration. In our study, muscle atrophy was most enhanced in curli-exposed hSOD1 male mice even though there wasn't more LMN degeneration (ChAT staining) in this group compared to vehicle or mutant *E. coli* exposed animals. LMN degeneration characteristic of ALS may not be the only preceding event to muscle degeneration and may occur independently, simultaneously or in reaction to muscle atrophy[55]. Additionally, curli-exposed mice exhibited significantly increased markers of inflammation in the brainstem as seen with our study in rats[18] and both bacterial-fed groups showed significant demyelination of the lumbar spinal cord.

We used a slow model of ALS progression to assess subtle early locomotive abnormalities with the TreadScan software. Standard measurements like RotaRod and inverted grid measure gross muscle weakness, which only develop after significant muscle atrophy has occurred. There were several differences in locomotion in hSOD1 male mice compared to WT as early as 4 months of age. It is well-established that males develop ALS sooner than females in humans[20], as well as in mouse models of ALS[56, 57], but the underlying mechanisms are not well understood. In our study, hSOD1 male mice displayed significantly increased proliferation of $CD19^+$ B cells, month 4 onwards compared to WT male mice, which did not occur in female hSOD1 mice. We hypothesize that this phenomenon may contribute to an earlier onset of ALS in males and warrants investigation. There were no significant effects of bacterial feeding (*E. coli*-curli and mutant) on B cell expression.

Administration of *E. coli* to mice for 6 months caused significant but silent dysbiosis, especially in male hSOD1 mice. However, there were no overt signs of ill-health measured regularly by body weight, general appearance, grooming habits, posture, and interaction with cage mates. Male hSOD1 mice fed with curli-producing *E. coli* showed a significant decrease in bacterial species diversity that was absent in mutant-fed (lacking curli) mice. Delivering this strain of *Proteobacteria* in the gut significantly suppressed colonization by other *Proteobacterial* strains. We did not detect a breach in gut barrier in any mice measured with FITC-Dextran administration at 6 months, contrary to a report of a leaky gut in hSOD1 G93A mice measured by ZO-1 protein expression[58].

In conclusion, chronic exposure to curli producing *E. coli* led to an earlier onset and faster progression of ALS. We hypothesize that interactions of curli with host MHC1 in the gut masked antigen presentation to T cells, leading to a suppressed adaptive immune response, evidenced by a significant decrease in peripheral immune response. This suggests that peripheral inflammation may be favorable in ALS. Conditions that prevent an optimal response of the adaptive immune system to fight ALS may lead to an

earlier or faster progression. We agree with Burberry et al[59] and Figueroa-Romero et al[60] that microbial influences outside of the nervous system are involved in ALS.

Strengths and Limitations

We developed a model of chronic gut dysbiosis by exposure to curli producing *E. co*li (*E. coli* WT), utilizing a slower onset ALS mouse model to enable early investigation of subtle motor abnormalities and monthly status of peripheral inflammation as ALS evolved. We also performed whole-genome shotgun sequencing to identify both bacterial and viral microbiota. We assessed the influence of expansion of *E. coli* in the gut in presence of mice's inherent microbiome, which is more clinically relevant than a germ-free model. Taken together, this study design may assist in identifying potential therapeutic approaches. The proposal that functional bacterial amyloids may be involved in ALS, has not been previously addressed. It is promising to note that the extensive similarities amongst the neurodegenerative disorders suggest strongly that similar molecular mechanisms are at play[40, 61]. Some of our data may differ from published studies of hSOD1 G93A mice that utilized a faster progression model. As shown by Sampson et al[62], polyphenols which inhibit bacterial amyloid aggregation in the gut in a mouse model of Parkinson's disease may be worth investigation in ALS. One of the most important limitations of this study was the inability to assess the influence of *E. coli* induced gut dysbiosis on full blown hind limb paralysis and survival of these mice. The sample size for histochemical analyses and qRT-PCR of the spinal cord and distal colon was small (n = 2–5) as groups were divided for fixed and frozen tissues.

Methods

Animals

Male and female SOD1-G93A mice (JAX 002299) were generated as previously described[17] This SOD1-G93A strain has a reduced copy number of the transgene as compared to the original strain and develops the ALS motor phenotype at six to seven months of age. Male SOD1-G93A founder mice were bred with C57BL/6J wild-type control mice. Transgenic mice and their littermate controls were housed in conventional, autoclaved ventilated caging.

Bacterial Strains and Characterizations

Escherichia coli strain BW25113 (WT) was first transformed with an empty plasmid containing an ampicillin resistance cassette (pET15b) as our selection marker and genotyped to confirm the presence of curli operon. *Escherichia coli* strain BW25113 csgGFED_BAC::FRT-kan-FRT (curli -) harbored a kanamycin resistance cassette and was genotyped to confirm knockout of the curli operon. These strains were cultured aerobically in LB media supplemented with each respective antibiotic marker at 37°C overnight. Ampicillin and kanamycin LB agar plates were inoculated and left to grow at room temperature

to further induce curli expression, confirmed via Western Blot analysis (data not shown). Plates were scraped and the bacterial strains were resuspended for feeding as described below.

Bacterial Preparation for Animal Feeding

The indicated bacterial strains were grown fresh for each feeding session and collected immediately prior to dosing. The bacterial strains were resuspended in 1.5% sodium bicarbonate in PBS (Phosphate Buffered Saline) and then mixed with the applesauce. The animals received ~10^9 CFU of bacteria per feeding session, three times per week over the course of 6 months. The animals were maintained on regular chow diet when not being fed bacterial strains. Confirmation of bacterial dosing was conducted by collecting fecal pellets and resuspending them in PBS and then plating them on each feeding group's respective ampicillin (BW25113 WT) or kanamycin (BW25113 Curli-) LB agar plates. Colonies were picked and genotyped as described below. Applesauce consumption was monitored after each feeding session to ensure proper dosing (data not shown). Body weights were monitored every other week and blood was collected from the submandibular vein monthly over the course of the study. All animal husbandry and experiments were approved by the University of Louisville's Institutional Animal Care and Use Committee (IACUC).

Rather than gavaging the mice three times per week, we provided a less stressful means of delivering bacteria to the mice via applesauce (adapted from Hsiao et al, Cell 2013[63]). The mice were fasted for two hours prior to feeding to encourage consumption of a novel substance. Upon weaning, all cage mates were acclimated to organic, unsweetened applesauce mixed with 1.5% sodium bicarbonate in PBS. The applesauce solution was spread over a food pellet placed in a sterile, micro-petri dish (35 x 10 mm "micro dish") and placed in an empty autoclaved cage free of bedding and food. After acclimation in a group setting, the mice were separated individually into autoclaved cages free of bedding and food pellets and were fed the applesauce solution similarly. Their individual consumption was monitored for two weeks with the last two sessions having applesauce without a food pellet. The mice tolerated the applesauce well and would typically consume all of it over the course of 4-6 hours.

Motor Function Assessment

For all motor assessments, each test utilized the same handlers, same blinded examiner and were conducted at the same time every month (3 weeks to 7 months). After each mouse, the assessment area was sprayed with 70% ethanol and wiped down. To reduce the odds of bacterial intermingling between groups, the three groups were run separately. Motor function were assessed using the following instruments: TreadScan and Basso Mouse Scale.

Motor Function Assessment - Treadmill Gait Kinematics (TreadScan)

Mice walking on a treadmill were recorded from below using a camera and TreadScan software as described previously[22]. Mice were first placed onto the treadmill and allowed to investigate the area for ~20 seconds to relax and get accustomed to the area. The treadmill is then turned on and the speed is slowly ramped up to allow the animals to get used to the task. The animals are then recorded for 2000 frames which is no more than 1 min. These videos allow analysis of the following 37 gait characteristics as well as Regularity Index and Plantar Stepping Index: stride time, stance length, stance length, stance time, swing time. brake time, propulsion time, percentage of stance, percentage of swing, stride length, average print area, max lateral deviation, minimum lateral deviation, mac longitudinal deviation, minimum longitudinal deviation, front track width, rear track width, left foot base, right foot base, instantaneous running speed, average running speed, overall running speed, absolute stride number, normalized stride number (stride frequency), homologous coupling, homolateral coupling, diagonal coupling, sciatic function index print length, sciatic function index toe spread, sciatic function index intermediary toe spread, sciatic function index print angle, gait angle, body rotation average, body rotation standard deviation, longitudinal movement average, lateral movement average, longitudinal movement standard deviation, lateral movement standard deviation, ratio index, coordinated pattern index and plantar stepping index.

Motor Function Assessment - Basso Mouse Scale (BMS)

BMS is a behavioral test which examines the involvement of the hindlimbs in locomotion[21]. The animals are gently removed from their home cages and placed in the bottom of an empty pool/livestock feeding trough. The animals are allowed to walk freely for a period of 4 minutes. During this time the animals are graded by a trained observer, and records were kept of limb movement, foot placement, coordination, trunk stability, and tail position during locomotion.

Intestinal Permeability Assay - FITC-Dextran

FITC-Dextran allows for the assessment of intestinal permeability and potential leaky gut. FITC-dextran (MW 4,000, Millipore-Sigma) was dissolved in PBS to yield a 60 mg/ml dosing solution concentration. Animals were fasted for 4 hours and then administered the FITC-dextran solution by oral gavage at a dose volume of 10 ml/kg. The animals were returned to their cages for 4 hours and then blood was collected from the submandibular vein. Serum was isolated, diluted, and measured with a plate reader (Ex/Em 485/530) Values were interpolated from a standard curve.

Whole-Gut Transit Time - Carmine Red

This test allows assessment of enteric nervous system or colonic abnormalities as described[64]. A 6% w/v carmine red (Millipore-Sigma) solution in 0.5% methylcellulose was produced. A dose volume of 10 ml/kg was used, and the solution was administered by oral gavage. After dosing, mice were moved to individual cages with white bedding and monitored every 30 mins for the appearance of the first red pellet for up to 8 hours post-dose. Times for each group were recorded, averaged, and compared for delay in whole-gut transit time between bacterial feeding groups.

SOD1 Pathology and Inflammatory Responses

Animals were anesthetized with isoflurane following institutional IACUC regulations and perfused with cold PBS and various tissues relevant to ALS were collected including skeletal muscle from hind limbs, spinal cord, distal colon, and brain. Skeletal muscle wet weights were recorded.

qRT-PCR

The tibialis anterior (TA) muscle and distal colon were homogenized, and RNA was extracted using an EZNA Total RNA kit (Omega Bio-Tek) according to manufacturer instructions. cDNA was made using high-capacity reverse transcription kit (Applied Biosystems) and qPCR was run on a CFX96 Real Time PCR system (BioRad) using SybrGreen master mix (Applied Biosystems). Primers utilized include the following: *beta Actin, TNFα, IL1b, MuRF1, Beclin, MAFBx, MUSA1, P62, PGC1a, Arginase1, EGR2, iNOS, CD38, TLR2, TLR4, IRAK4, Myd88, ZO-1, Lipocalin-2, IL6, IL22, NLRP3, IL23, Foxp3, IFNγ, NOX1, MMP9.* Please see the table for primer sequences. Results are reported using the ΔΔCT method.

Western blot analysis

The tibialis anterior muscle, distal colon, and brain were homogenized in RIPA buffer and protein concentrations were measured using BCA (bicinchoninic acid) assay (Pierce 23225). The following antibodies were used hSOD1 G93A (SOD1 MS785, GTX57211), TNFa (ABclonal A0277) and beta-Actin (ABclonal AC026).

Immunohistochemistry

The tibialis anterior muscle, distal colon, lumbar spinal cord, and brain were post-fixed in 10% neutral buffered formalin for 48 hours and then switched to 70% ethanol until ready for embedding with paraffin.

Paraffin embedded samples were cut into 6-8um sections on slides for staining. Tissue sections were deparaffinized, rehydrated and probed with the following antibodies: hSOD1 (SOD1 MS785, GTX57211), ChAT (ProteinTech, 20747-1-AP), GFAP (ABclonal, A10873), Iba1 (Abcam, ab17886), Histochemistry was performed using antigen retrieval with citric acid buffer at 95C for 30 mins and Vector ABC and NovaRed substrate system according to manufacturer instructions (Vector Laboratories). Please refer to the table for additional antibody information. Luxol Fast Blue (LFB) and eosin stain of the spinal cord were performed by the Dept. of Patholollgy at University of Louisville. Slides were scanned using an Aperio Slide Scanner (Leica Biosystems). Images were quantified in ImageJ using optical density, mean gray value, or % area depending on context, described in figure legends.

FACS analyses

FACS analysis were performed every month (3 weeks onwards up to 7 months). Blood was collected (100-200ul) using a small needle prick in the submandibular vein in EDTA collection tubes. 50ul blood was utilized for immunophenotyping. RBCs were lysed/fixed (Biolegend 422401), followed by incubation with immunofluorescent antibodies for the following: CD3 (BD Biosciences 557724), CD4 (Biolegend 100406), CD8 (BD Biosciences 564297), CD19 (BD Biosciences 562291), NK cells (NK1.1 BD Biosciences 557391), CD11b (BD Biosciences 563402), Ly6G (BD Biosciences 561236), Ly6C (BD Biosciences 560596), CD11c (BD Biosciences 550261). Post-processing, samples were stored at 4C in dark for 3-4 days, until running on a BD multicolor LSR Fortessa. Data were analyzed using Flow Jo^{TM} 10.5.3.

Cytokine Multiplex

Cytokine multiplex were probed for three time points - 3 weeks, 3 months, and 6 months. Blood samples were spun down in their respective EDTA tubes at 1,000xG for 10 minutes and plasma was collected and stored at -80º C until ready to be shipped. 25ul samples were diluted two-fold in PBS and shipped on dry ice for a mouse cytokine 32-plex using a BioPlex 200 Mouse Cytokine Array (Eve Technologies).

Fecal metagenomics

Fecal pellets were collected and stored at -80C and shipped on dry ice to CosmosID Metagenomics, Rockville, MD. DNA extraction, Illumina library preparation, sequencing at 3 million total reads (1x150bp or 2x150) were performed at CosmosID. PCA plots, alpha and beta diversity PCoA were constructed utilizing the Cosmos ID Metagenomics App platform. Linear discriminant analysis Effect Size (LEfSE) and relative abundance analyses were performed by our in-house bioinformatician.

Key Resources Table

Reagent Type, Species, or Resource	Designation	Source or Reference	Identifiers	Additional Information
Strain, strain background (*Mus musculus*)	B6.Cg-Tg(SOD1*G93A)dl1Gur/J, C57BL/6J background	The Jackson Lab	SOD1-G93A	*17*
Strain, strain background (*Escherichia coli*)	Str. BW25113, rrnB3 ΔlacZ4787 hsdR514 Δ(araBAD)567 Δ(rhaBAD)568 rph-1	Matthew R. Chapman	WT (wild-type)	*65*
Strain, strain background (*Escherichia coli*)	Str. BW25113, csgGFED_BAC::FRT-kan-FRT	Matthew R. Chapman	Curli-	*65*
Sequence Based Reagent	*hSOD1:* 5'-GGGAAGCTGTTGTCCCAAG-3' And 5'-CAAGGGGAGGTAAAAGAGAGC-3'	Integrated DNA Technologies	gDNA, qPCR Primer	The Jackson Labs
Sequence Based Reagent	*ApoB*, Internal Positive Control: 5'-CACGTGGGCTCCAGCATT-3' And 5'-TCACCAGTCATTTCTGCCTTTG-3'	IDT	gDNA, qPCR Primer	The Jackson Labs
Sequence Based Reagent	*csgA:* 5'-GATCTGACCCAACGTGGCTTCG-3' And 5'- GATGAGCGGTCGCGTTGTTACC-3'	IDT	gDNA, PCR Primer	
Sequence Based Reagent	*csgC:* 5'-CCTGTTTTTTTTCGGGAGAAGAATATG-3' And 5'-ATTCATCTTATGCTCGATATTTCAACAA-3'	IDT	gDNA, PCR Primer	
Sequence Based Reagent	*csgB:* 5'-ACCAGGTCCAGGGTGACAACATG-3'	IDT	gDNA, PCR Primer	

	And 5’-AGTCGAATGGAAATTAACGTTGTGTC-3’			
Sequence Based Reagent	*csgD:* 5’-ACCAGGTCCAGGGTGACAACATG-3’ And 5’-AGTCGAATGGAAATTAACGTTGTGTC-3’	IDT	gDNA, PCR Primer	
Sequence Based Reagent	*csgE:* 5’-TTTTTATTTAGAATTCATCATGCGCCAA-3’ And 5’-ATAACCTCAGGCGATAAAGCCATG-3’	IDT	gDNA, PCR Primer	
Sequence Based Reagent	*csgF:* 5’-GGGGCTTAAAAATCGGTTGAGTTATT-3’ And 5’-TAAAAAATTGTTCGGAGGCTGCAATG-3’	IDT	gDNA, PCR Primer	
Sequence Based Reagent	*csgG:* 5’-TGTCAGGATTCCGGTGGAACCGA-3’ And 5’-CCCAGCTTCATAAGGAAAATAATCATG-3’	IDT	gDNA, PCR Primer	
Sequence Based Reagent	*ycdZ:* 5’-GAACATACTTCTCTCTATTGCAATCA-3’	IDT	gDNA, PCR Primer	
Sequence Based Reagent	*ymdA:* 5’-CAAACTGCCGAGCATAAGAGAG-3’	IDT	gDNA, PCR Primer	
Sequence Based Reagent	*Beta actin:* 5’-GGCTGTATTCCCCTCCATCG-3’ And 5’-CCAGTTGGTAACAATGCCATGT-3’	IDT	cDNA, PCR Primer	PrimerBank

Sequence Based Reagent	*MAFBx:* 5’-CAGCTTCGTGAGCGACCTC-3’ And 5’-GGCAGTCGAGAAGTCCAGTC-3’	IDT	cDNA, PCR Primer	PrimerBank
Sequence Based Reagent	*MuRF1:* 5’-GTGTGAGGTGCCTACTTGCTC-3’ And 5’-GCTCAGTCTTCTGTCCTTGGA-3’	IDT	cDNA, PCR Primer	PrimerBank
Sequence Based Reagent	*MUSA1:* 5’-TATGAACTGTGTCAGTAGACGGT-3’ And 5’-CGATGTTCGTCAGCTTTACAAGA-3’	IDT	cDNA, PCR Primer	PrimerBank
Sequence Based Reagent	*Beclin 1:* 5’-ATGGAGGGGTCTAAGGCGTC-3’ And 5’-TCCTCTCCTGAGTTAGCCTCT-3’	IDT	cDNA, PCR Primer	PrimerBank
Sequence Based Reagent	*P62:* 5’-AGGATGGGGACTTGGTTGC-3’ And 5’-TCACAGATCACATTGGGGTGC-3’	IDT	cDNA, PCR Primer	PrimerBank
Sequence Based Reagent	*PGC1-alpha:* 5’-TATGGAGTGACATAGAGTGTGCT-3’ And 5’-CCACTTCAATCCACCCAGAAAG-3’	IDT	cDNA, PCR Primer	PrimerBank
Sequence Based Reagent	*TNF-alpha:* 5’-CAGGCGGTGCCTATGTCTC-3’ And 5’-CGATCACCCCGAAGTTCAGTAG-3’	IDT	cDNA, PCR Primer	PrimerBank
Sequence Based Reagent	*IL-1b:* 5’-TTCAGGCAGGCAGTATCACTC-3’	IDT	cDNA, PCR Primer	PrimerBank

	And 5’-GAAGGTCCACGGGAAAGACAC-3’			
Sequence Based Reagent	*ZO-1:* 5’-GCTTTAGCGAACAGAAGGAGC-3’ And 5’-TTCATTTTTCCGAGACTTCACCA-3’	IDT	cDNA, PCR Primer	PrimerBank
Sequence Based Reagent	*TLR2:* 5’-GCAAACGCTGTTCTGCTCAG-3’ And 5’-AGGCGTCTCCCTCTATTGTATT-3’	IDT	cDNA, PCR Primer	PrimerBank
Sequence Based Reagent	*TLR4:* 5’-GCCTTTCAGGGAATTAAGCTCC-3’ And 5’-GATCAACCGATGGACGTGTAAA-3’	IDT	cDNA, PCR Primer	PrimerBank
Sequence Based Reagent	*IRAK4:* 5’-CCGGCGACGACAGATACAATC-3’ And 5’-TCTGGACCAGTAGATCCACAAG-3’	IDT	cDNA, PCR Primer	PrimerBank
Sequence Based Reagent	*MyD88:* 5’-AGGACAAACGCCGGAACTTTT-3’ And 5’-GCCGATAGTCTGTCTGTTCTAGT-3’	IDT	cDNA, PCR Primer	PrimerBank
Sequence Based Reagent	*Lipocalin-2:* 5’-TGGCCCTGAGTGTCATGTG-3’ And 5’-CTCTTGTAGCTCATAGATGGTGC-3’	IDT	cDNA, PCR Primer	PrimerBank
Sequence Based Reagent	*CD38:* 5’-TCCCTCCGTGAGCCATTTTAC-3’ And 5’-CGATGTCGTGCATCACCCA-3’	IDT	cDNA, PCR Primer	PrimerBank

Sequence Based Reagent	*EGR2:* 5’-GCCAAGGCCGTAGACAAAATC-3’ And 5’-CCACTCCGTTCATCTGGTCA-3’	IDT	cDNA, PCR Primer	PrimerBank
Sequence Based Reagent	*Arginase-1:* 5’-CTCCAAGCCAAAGTCCTTAGAG-3’ And 5’-AGGAGCTGTCATTAGGGACATC-3’	IDT	cDNA, PCR Primer	PrimerBank
Sequence Based Reagent	*iNOS:* 5’-GTTCTCAGCCCAACAATACAAGA-3’ And 5’-GTGGACGGGTCGATGTCAC-3’	IDT	cDNA, PCR Primer	PrimerBank
Sequence Based Reagent	*NLRP3:* 5’-ATTACCCGCCCGAGAAAGG-3’ And 5’-TCGCAGCAAAGATCCACACAG-3’	IDT	cDNA, PCR Primer	PrimerBank
Sequence Based Reagent	*IL-6:* 5’-TAGTCCTTCCTACCCCAATTTCC-3’ And 5’-TTGGTCCTTAGCCACTCCTTC-3’	IDT	cDNA, PCR Primer	PrimerBank
Sequence Based Reagent	*IL-22:* 5’-ATGAGTTTTTCCCTTATGGGGAC-3’ And 5’-GCTGGAAGTTGGACACCTCAA-3’	IDT	cDNA, PCR Primer	PrimerBank
Sequence Based Reagent	*IL-23a:* 5’-ATGCTGGATTGCAGAGCAGTA-3’ And 5’-ACGGGGCACATTATTTTTAGTCT-3’	IDT	cDNA, PCR Primer	PrimerBank
Sequence Based Reagent	*NOX1:* 5’-GGTTGGGGCTGAACATTTTTC-3’	IDT	cDNA, PCR Primer	PrimerBank

	And 5’-TCGACACACAGGAATCAGGAT-3’			
Sequence Based Reagent	*MMP9:* 5’-GGACCCGAAGCGGACATTG-3’ And 5’-CGTCGTCGAAATGGGCATCT-3’	IDT	cDNA, PCR Primer	PrimerBank
Sequence Based Reagent	*FoxP3:* 5’-ACCATTGGTTTACTCGCATGT-3’ And 5’-TCCACTCGCACAAAGCACTT-3’	IDT	cDNA, PCR Primer	PrimerBank
Sequence Based Reagent	*IFN-gamma:* 5’-ATGAACGCTACACACTGCATC-3’ And 5’-CCATCCTTTTGCCAGTTCCTC-3’	IDT	cDNA, PCR Primer	PrimerBank

Declarations

Author Contributions

RPF conceptualized the idea and hypothesis.

ZK, JDM, RPF, LJB, LJS designed the study and experiments, provided feedback and discussion.

ZK and JDM performed the experiments and data analyses.

RS performed the bioinformatics analysis of shotgun sequencing.

JM performed monthly motor assessments.

DAB conducted statistical analyses on all motor assessments.

SMS assisted with immunohistochemistry.

ED analyzed distal colon morphology.

Funding

Supported in part by Axial Biotherapeutics, Jewish Heritage Fund for Excellence, the family of E.A. Ford III, Dr Walter Cowan and the University of Louisville.

Competing Interests Statement

The authors have no disclosures.

References

1. Trojsi, F., Monsurro, M. R., and Tedeschi, G. (2013) Exposure to environmental toxicants and pathogenesis of amyotrophic lateral sclerosis: state of the art and research perspectives, *Int J Mol Sci 14*, 15286–15311.
2. Saffouri, G. B., Shields-Cutler, R. R., Chen, J., Yang, Y., Lekatz, H. R., Hale, V. L., Cho, J. M., Battaglioli, E. J., Bhattarai, Y., Thompson, K. J., Kalari, K. K., Behera, G., Berry, J. C., Peters, S. A., Patel, R., Schuetz, A. N., Faith, J. J., Camilleri, M., Sonnenburg, J. L., Farrugia, G., Swann, J. R., Grover, M., Knights, D., and Kashyap, P. C. (2019) Small intestinal microbial dysbiosis underlies symptoms associated with functional gastrointestinal disorders, *Nature communications 10*, 2012.
3. Yu, L. X., and Schwabe, R. F. (2017) The gut microbiome and liver cancer: mechanisms and clinical translation, *Nature reviews. Gastroenterology & hepatology 14*, 527–539.
4. Wang, L., Zhou, J., Xin, Y., Geng, C., Tian, Z., Yu, X., and Dong, Q. (2016) Bacterial overgrowth and diversification of microbiota in gastric cancer, *Eur J Gastroenterol Hepatol 28*, 261–266.
5. Vipperla, K., and O'Keefe, S. J. (2012) The microbiota and its metabolites in colonic mucosal health and cancer risk, *Nutr Clin Pract 27*, 624–635.
6. Alibhai, J., Blanco, R. A., Barria, M. A., Piccardo, P., Caughey, B., Perry, V. H., Freeman, T. C., and Manson, J. C. (2016) Distribution of Misfolded Prion Protein Seeding Activity Alone Does Not Predict Regions of Neurodegeneration, *PLoS biology 14*, e1002579.
7. Blacher, E., Bashiardes, S., Shapiro, H., Rothschild, D., Mor, U., Dori-Bachash, M., Kleimeyer, C., Moresi, C., Harnik, Y., Zur, M., Zabari, M., Brik, R. B., Kviatcovsky, D., Zmora, N., Cohen, Y., Bar, N., Levi, I., Amar, N., Mehlman, T., Brandis, A., Biton, I., Kuperman, Y., Tsoory, M., Alfahel, L., Harmelin, A., Schwartz, M., Israelson, A., Arike, L., Johansson, M. E. V., Hansson, G. C., Gotkine, M., Segal, E., and Elinav, E. (2019) Potential roles of gut microbiome and metabolites in modulating ALS in mice, *Nature 572*, 474–480.
8. Zhang, Y. G., Wu, S., Yi, J., Xia, Y., Jin, D., Zhou, J., and Sun, J. (2017) Target Intestinal Microbiota to Alleviate Disease Progression in Amyotrophic Lateral Sclerosis, *Clin Ther 39*, 322–336.
9. Sampson, T. R., Challis, C., Jain, N., Moiseyenko, A., Ladinsky, M. S., Shastri, G. G., Thron, T., Needham, B. D., Horvath, I., Debelius, J. W., Janssen, S., Knight, R., Wittung-Stafshede, P., Gradinaru,

V., Chapman, M., and Mazmanian, S. K. (2020) A gut bacterial amyloid promotes alpha-synuclein aggregation and motor impairment in mice, *Elife 9*.

10. Rapsinski, G. J., Newman, T. N., Oppong, G. O., van Putten, J. P., and Tukel, C. (2013) CD14 protein acts as an adaptor molecule for the immune recognition of Salmonella curli fibers, *J Biol Chem 288*, 14178–14188.
11. Tukel, C., Nishimori, J. H., Wilson, R. P., Winter, M. G., Keestra, A. M., van Putten, J. P., and Baumler, A. J. (2010) Toll-like receptors 1 and 2 cooperatively mediate immune responses to curli, a common amyloid from enterobacterial biofilms, *Cellular microbiology 12*, 1495–1505.
12. Rapsinski, G. J., Wynosky-Dolfi, M. A., Oppong, G. O., Tursi, S. A., Wilson, R. P., Brodsky, I. E., and Tukel, C. (2015) Toll-like receptor 2 and NLRP3 cooperate to recognize a functional bacterial amyloid, curli, *Infect Immun 83*, 693–701.
13. Olsen, A., Wick, M. J., Morgelin, M., and Bjorck, L. (1998) Curli, fibrous surface proteins of Escherichia coli, interact with major histocompatibility complex class I molecules, *Infection and immunity 66*, 944–949.
14. Dueholm, M. S., Nielsen, S. B., Hein, K. L., Nissen, P., Chapman, M., Christiansen, G., Nielsen, P. H., and Otzen, D. E. (2011) Fibrillation of the major curli subunit CsgA under a wide range of conditions implies a robust design of aggregation, *Biochemistry 50*, 8281–8290.
15. Perov, S., Lidor, O., Salinas, N., Golan, N., Tayeb-Fligelman, E., Deshmukh, M., Willbold, D., and Landau, M. (2019) Structural Insights into Curli CsgA Cross-beta Fibril Architecture Inspire Repurposing of Anti-amyloid Compounds as Anti-biofilm Agents, *PLoS Pathog 15*, e1007978.
16. Alam, P., Bousset, L., Melki, R., and Otzen, D. E. (2019) alpha-synuclein oligomers and fibrils: a spectrum of species, a spectrum of toxicities, *J Neurochem 150*, 522–534.
17. Gurney, M. E., Pu, H., Chiu, A. Y., Dal Canto, M. C., Polchow, C. Y., Alexander, D. D., Caliendo, J., Hentati, A., Kwon, Y. W., Deng, H. X., and et al. (1994) Motor neuron degeneration in mice that express a human Cu,Zn superoxide dismutase mutation, *Science 264*, 1772–1775.
18. Chen, S. G., Stribinskis, V., Rane, M. J., Demuth, D. R., Gozal, E., Roberts, A. M., Jagadapillai, R., Liu, R., Choe, K., Shivakumar, B., Son, F., Jin, S., Kerber, R., Adame, A., Masliah, E., and Friedland, R. P. (2016) Exposure to the Functional Bacterial Amyloid Protein Curli Enhances Alpha-Synuclein Aggregation in Aged Fischer 344 Rats and Caenorhabditis elegans, *Scientific reports 6*, 34477.
19. Baba, T., Ara, T., Hasegawa, M., Takai, Y., Okumura, Y., Baba, M., Datsenko, K. A., Tomita, M., Wanner, B. L., and Mori, H. (2006) Construction of Escherichia coli K-12 in-frame, single-gene knockout mutants: the Keio collection, *Mol Syst Biol 2*, 2006 0008.
20. McCombe, P. A., and Henderson, R. D. (2010) Effects of gender in amyotrophic lateral sclerosis, *Gend Med 7*, 557–570.
21. Basso, D. M., Fisher, L. C., Anderson, A. J., Jakeman, L. B., McTigue, D. M., and Popovich, P. G. (2006) Basso Mouse Scale for locomotion detects differences in recovery after spinal cord injury in five common mouse strains, *Journal of neurotrauma 23*, 635–659.

22. Beare, J. E., Morehouse, J. R., DeVries, W. H., Enzmann, G. U., Burke, D. A., Magnuson, D. S., and Whittemore, S. R. (2009) Gait analysis in normal and spinal contused mice using the TreadScan system, *Journal of neurotrauma 26*, 2045–2056.
23. Philips, T., and Rothstein, J. D. (2014) Glial cells in amyotrophic lateral sclerosis, *Experimental neurology 262 Pt B*, 111–120.
24. Sabat, R., Ouyang, W., and Wolk, K. (2014) Therapeutic opportunities of the IL-22-IL-22R1 system, *Nat Rev Drug Discov 13*, 21–38.
25. Jinquan, T., Quan, S., Feili, G., Larsen, C. G., and Thestrup-Pedersen, K. (1999) Eotaxin activates T cells to chemotaxis and adhesion only if induced to express CCR3 by IL-2 together with IL-4, *J Immunol 162*, 4285–4292.
26. Gerber, B. O., Zanni, M. P., Uguccioni, M., Loetscher, M., Mackay, C. R., Pichler, W. J., Yawalkar, N., Baggiolini, M., and Moser, B. (1997) Functional expression of the eotaxin receptor CCR3 in T lymphocytes co-localizing with eosinophils, *Curr Biol 7*, 836–843.
27. Fife, B. T., Kennedy, K. J., Paniagua, M. C., Lukacs, N. W., Kunkel, S. L., Luster, A. D., and Karpus, W. J. (2001) CXCL10 (IFN-gamma-inducible protein-10) control of encephalitogenic CD4 + T cell accumulation in the central nervous system during experimental autoimmune encephalomyelitis, *J Immunol 166*, 7617–7624.
28. Pertl, U., Luster, A. D., Varki, N. M., Homann, D., Gaedicke, G., Reisfeld, R. A., and Lode, H. N. (2001) IFN-γ-inducible protein-10 is essential for the generation of a protective tumor-specific CD8 T cell response induced by single-chain IL-12 gene therapy, *The Journal of Immunology 166*, 6944–6951.
29. Sampson, T. R., Debelius, J. W., Thron, T., Janssen, S., Shastri, G. G., Ilhan, Z. E., Challis, C., Schretter, C. E., Rocha, S., Gradinaru, V., Chesselet, M. F., Keshavarzian, A., Shannon, K. M., Krajmalnik-Brown, R., Wittung-Stafshede, P., Knight, R., and Mazmanian, S. K. (2016) Gut Microbiota Regulate Motor Deficits and Neuroinflammation in a Model of Parkinson's Disease, *Cell 167*, 1469–1480.e1412.
30. Di Gioia, D., Bozzi Cionci, N., Baffoni, L., Amoruso, A., Pane, M., Mogna, L., Gaggia, F., Lucenti, M. A., Bersano, E., Cantello, R., De Marchi, F., and Mazzini, L. (2020) A prospective longitudinal study on the microbiota composition in amyotrophic lateral sclerosis, *BMC Med 18*, 153.
31. Mazzini, L., Mogna, L., De Marchi, F., Amoruso, A., Pane, M., Aloisio, I., Cionci, N. B., Gaggia, F., Lucenti, A., Bersano, E., Cantello, R., Di Gioia, D., and Mogna, G. (2018) Potential Role of Gut Microbiota in ALS Pathogenesis and Possible Novel Therapeutic Strategies, *J Clin Gastroenterol 52 Suppl 1, Proceedings from the 9th Probiotics, Prebiotics and New Foods, Nutraceuticals and Botanicals for Nutrition & Human and Microbiota Health Meeting, held in Rome, Italy from September 10 to 12, 2017*, S68-S70.
32. Rowin, J., Xia, Y., Jung, B., and Sun, J. (2017) Gut inflammation and dysbiosis in human motor neuron disease, *Physiol Rep 5*.
33. Harach, T., Marungruang, N., Duthilleul, N., Cheatham, V., Mc Coy, K. D., Frisoni, G., Neher, J. J., Fak, F., Jucker, M., Lasser, T., and Bolmont, T. (2017) Reduction of Abeta amyloid pathology in APPPS1 transgenic mice in the absence of gut microbiota, *Scientific reports 7*, 41802.

34. Kowalski, K., and Mulak, A. (2019) Brain-Gut-Microbiota Axis in Alzheimer's Disease, *J Neurogastroenterol Motil 25*, 48–60.
35. Li, Y., Luo, Z. Y., Hu, Y. Y., Bi, Y. W., Yang, J. M., Zou, W. J., Song, Y. L., Li, S., Shen, T., Li, S. J., Huang, L., Zhou, A. J., Gao, T. M., and Li, J. M. (2020) The gut microbiota regulates autism-like behavior by mediating vitamin B6 homeostasis in EphB6-deficient mice, *Microbiome 8*, 120.
36. Sharon, G., Cruz, N. J., Kang, D. W., Gandal, M. J., Wang, B., Kim, Y. M., Zink, E. M., Casey, C. P., Taylor, B. C., Lane, C. J., Bramer, L. M., Isern, N. G., Hoyt, D. W., Noecker, C., Sweredoski, M. J., Moradian, A., Borenstein, E., Jansson, J. K., Knight, R., Metz, T. O., Lois, C., Geschwind, D. H., Krajmalnik-Brown, R., and Mazmanian, S. K. (2019) Human Gut Microbiota from Autism Spectrum Disorder Promote Behavioral Symptoms in Mice, *Cell 177*, 1600–1618 e1617.
37. Valles-Colomer, M., Falony, G., Darzi, Y., Tigchelaar, E. F., Wang, J., Tito, R. Y., Schiweck, C., Kurilshikov, A., Joossens, M., Wijmenga, C., Claes, S., Van Oudenhove, L., Zhernakova, A., Vieira-Silva, S., and Raes, J. (2019) The neuroactive potential of the human gut microbiota in quality of life and depression, *Nat Microbiol 4*, 623–632.
38. Abenavoli, L., Scarpellini, E., Colica, C., Boccuto, L., Salehi, B., Sharifi-Rad, J., Aiello, V., Romano, B., De Lorenzo, A., Izzo, A. A., and Capasso, R. (2019) Gut Microbiota and Obesity: A Role for Probiotics, *Nutrients 11*.
39. Glassner, K. L., Abraham, B. P., and Quigley, E. M. M. (2020) The microbiome and inflammatory bowel disease, *J Allergy Clin Immunol 145*, 16–27.
40. Friedland, R. P. (2015) Mechanisms of molecular mimicry involving the microbiota in neurodegeneration, *J Alzheimers Dis 45*, 349–362.
41. Friedland, R. P., and Chapman, M. R. (2017) The role of microbial amyloid in neurodegeneration, *PLoS Pathog 13*, e1006654.
42. Beers, D. R., Zhao, W., Wang, J., Zhang, X., Wen, S., Neal, D., Thonhoff, J. R., Alsuliman, A. S., Shpall, E. J., Rezvani, K., and Appel, S. H. (2017) ALS patients' regulatory T lymphocytes are dysfunctional, and correlate with disease progression rate and severity, *JCI insight 2*, e89530.
43. Mantovani, S., Garbelli, S., Pasini, A., Alimonti, D., Perotti, C., Melazzini, M., Bendotti, C., and Mora, G. (2009) Immune system alterations in sporadic amyotrophic lateral sclerosis patients suggest an ongoing neuroinflammatory process, *J Neuroimmunol 210*, 73–79.
44. Henkel, J. S., Beers, D. R., Wen, S., Rivera, A. L., Toennis, K. M., Appel, J. E., Zhao, W., Moore, D. H., Powell, S. Z., and Appel, S. H. (2013) Regulatory T-lymphocytes mediate amyotrophic lateral sclerosis progression and survival, *EMBO Mol Med 5*, 64–79.
45. McCombe, P. A., Lee, J. D., Woodruff, T. M., and Henderson, R. D. (2020) The Peripheral Immune System and Amyotrophic Lateral Sclerosis, *Frontiers in neurology 11*, 279.
46. Thonhoff, J. R., Beers, D. R., Zhao, W., Pleitez, M., Simpson, E. P., Berry, J. D., Cudkowicz, M. E., and Appel, S. H. (2018) Expanded autologous regulatory T-lymphocyte infusions in ALS: A phase I, first-in-human study, *Neurology(R) neuroimmunology & neuroinflammation 5*, e465.

47. Xie, Y., Zhou, B., Lin, M. Y., Wang, S., Foust, K. D., and Sheng, Z. H. (2015) Endolysosomal Deficits Augment Mitochondria Pathology in Spinal Motor Neurons of Asymptomatic fALS Mice, *Neuron 87*, 355–370.
48. Settembre, C., and Ballabio, A. (2011) TFEB regulates autophagy: an integrated coordination of cellular degradation and recycling processes, *Autophagy 7*, 1379–1381.
49. Murton, A. J., Constantin, D., and Greenhaff, P. L. (2008) The involvement of the ubiquitin proteasome system in human skeletal muscle remodelling and atrophy, *Biochim Biophys Acta 1782*, 730–743.
50. von Grabowiecki, Y., Abreu, P., Blanchard, O., Palamiuc, L., Benosman, S., Meriaux, S., Devignot, V., Gross, I., Mellitzer, G., and de Aguilar, J. L. G. (2016) Transcriptional activator TAp63 is upregulated in muscular atrophy during ALS and induces the pro-atrophic ubiquitin ligase Trim63, *Elife 5*, e10528.
51. Léger, B., Vergani, L., Sorarù, G., Hespel, P., Derave, W., Gobelet, C., D'Ascenzio, C., Angelini, C., and Russell, A. P. (2006) Human skeletal muscle atrophy in amyotrophic lateral sclerosis reveals a reduction in Akt and an increase in atrogin-1, *The FASEB journal 20*, 583–585.
52. Sartori, R., Schirwis, E., Blaauw, B., Bortolanza, S., Zhao, J., Enzo, E., Stantzou, A., Mouisel, E., Toniolo, L., and Ferry, A. (2013) BMP signaling controls muscle mass, *Nature genetics 45*, 1309–1318.
53. Bodine, S. C., and Baehr, L. M. (2014) Skeletal muscle atrophy and the E3 ubiquitin ligases MuRF1 and MAFbx/atrogin-1, *American Journal of Physiology-Endocrinology and Metabolism 307*, E469-E484.
54. Dobrowolny, G., Aucello, M., Rizzuto, E., Beccafico, S., Mammucari, C., Bonconpagni, S., Belia, S., Wannenes, F., Nicoletti, C., and Del Prete, Z. (2008) Skeletal muscle is a primary target of SOD1G93A-mediated toxicity, *Cell metabolism 8*, 425–436.
55. Pikatza-Menoio, O., Elicegui, A., Bengoetxea, X., Naldaiz-Gastesi, N., Lopez de Munain, A., Gerenu, G., Gil-Bea, F. J., and Alonso-Martin, S. (2021) The Skeletal Muscle Emerges as a New Disease Target in Amyotrophic Lateral Sclerosis, *J Pers Med 11*.
56. Trieu, V. N., and Uckun, F. M. (1999) Genistein is neuroprotective in murine models of familial amyotrophic lateral sclerosis and stroke, *Biochemical and biophysical research communications 258*, 685–688.
57. Veldink, J., Bär, P., Joosten, E., Otten, M., Wokke, J., and Van den Berg, L. (2003) Sexual differences in onset of disease and response to exercise in a transgenic model of ALS, *Neuromuscular Disorders 13*, 737–743.
58. Wu, S., Yi, J., Zhang, Y. G., Zhou, J., and Sun, J. (2015) Leaky intestine and impaired microbiome in an amyotrophic lateral sclerosis mouse model, *Physiol Rep 3*.
59. Burberry, A., Wells, M. F., Limone, F., Couto, A., Smith, K. S., Keaney, J., Gillet, G., van Gastel, N., Wang, J. Y., Pietilainen, O., Qian, M., Eggan, P., Cantrell, C., Mok, J., Kadiu, I., Scadden, D. T., and Eggan, K. (2020) C9orf72 suppresses systemic and neural inflammation induced by gut bacteria, *Nature 582*, 89–94.
60. Figueroa-Romero, C., Guo, K., Murdock, B. J., Paez-Colasante, X., Bassis, C. M., Mikhail, K. A., Raue, K. D., Evans, M. C., Taubman, G. F., McDermott, A. J., O'Brien, P. D., Savelieff, M. G., Hur, J., and Feldman,

E. L. (2019) Temporal evolution of the microbiome, immune system and epigenome with disease progression in ALS mice, *Disease models & mechanisms 13*.

61. Miraglia, F., and Colla, E. (2019) Microbiome, Parkinson's Disease and Molecular Mimicry, *Cells 8*.
62. (!!! INVALID CITATION !!! 26).
63. Hsiao, E. Y., McBride, S. W., Hsien, S., Sharon, G., Hyde, E. R., McCue, T., Codelli, J. A., Chow, J., Reisman, S. E., Petrosino, J. F., Patterson, P. H., and Mazmanian, S. K. (2013) Microbiota modulate behavioral and physiological abnormalities associated with neurodevelopmental disorders, *Cell 155*, 1451–1463.
64. Kuo, Y. M., Li, Z., Jiao, Y., Gaborit, N., Pani, A. K., Orrison, B. M., Bruneau, B. G., Giasson, B. I., Smeyne, R. J., Gershon, M. D., and Nussbaum, R. L. (2010) Extensive enteric nervous system abnormalities in mice transgenic for artificial chromosomes containing Parkinson disease-associated alpha-synuclein gene mutations precede central nervous system changes, *Hum Mol Genet 19*, 1633–1650.
65. Smith, D. R., Price, J. E., Burby, P. E., Blanco, L. P., Chamberlain, J., and Chapman, M. R. (2017) The Production of Curli Amyloid Fibers Is Deeply Integrated into the Biology of Escherichia coli, *Biomolecules 7*.

Figures

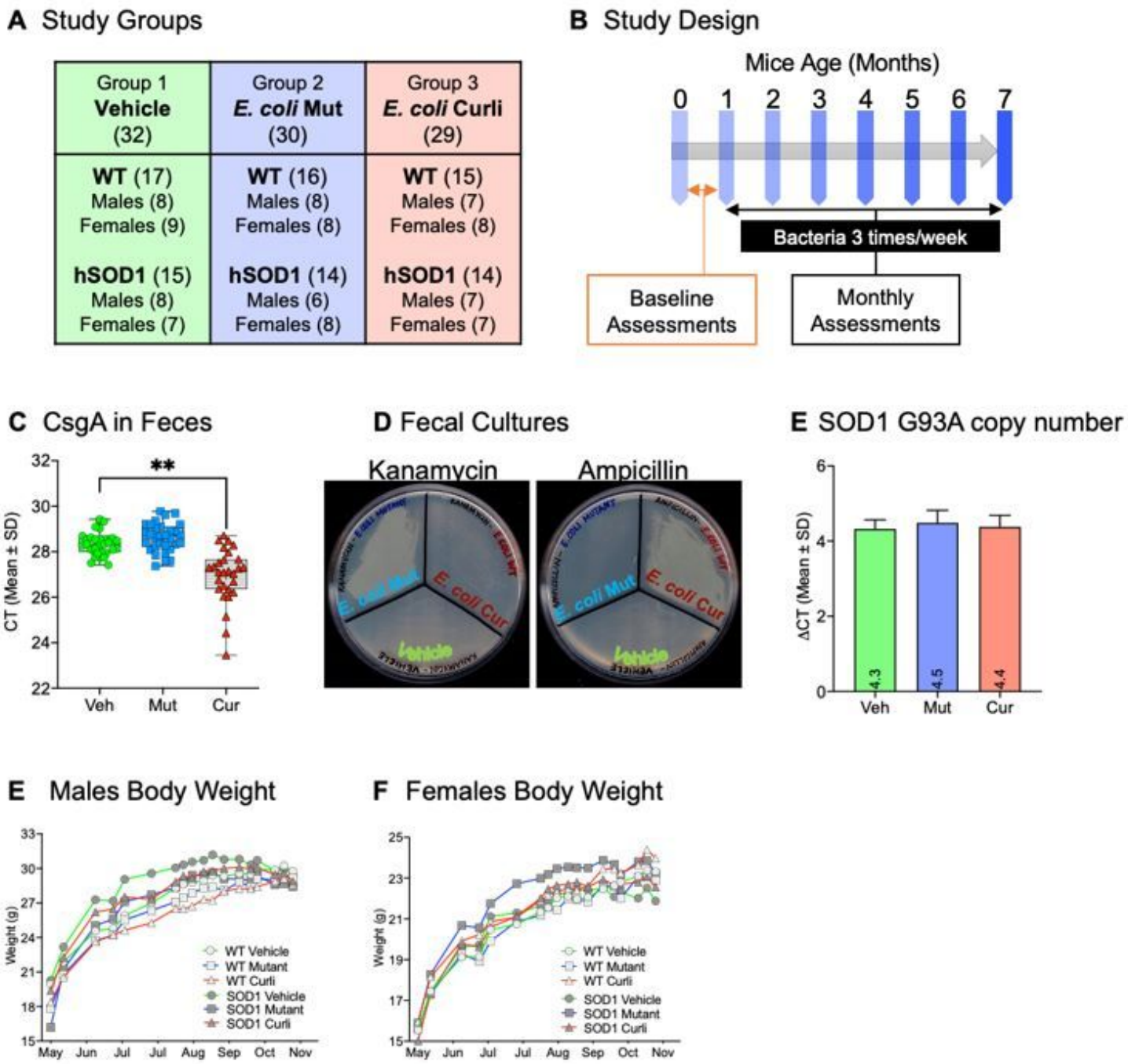

Figure 1

Study Design (A) There were a total of 91 animals in 3 main experimental groups – Group 1: Vehicle (applesauce only), Group 2: E. coli mutant in applesauce (lacking CsgA gene), Group 3: E. coli WT in applesauce (CsgA/curli producing). (B) Study design: Mice were assessed at baseline (3 weeks of age) and monthly for several functional measures. Feeding of bacteria or vehicle was started at 1 month of age, three times/week, for 6 months. (C) Confirmation of feeding - fecal pellets collected on a non-bacterial feeding day at 6 months were evaluated for presence of bacterial CsgA gene. qPCR detected overexpression of CsgA in the curli-fed group, as well as basal endogenous expression in the Veh and

Mut groups **p<0.001 One-way ANOVA. (D) Confirmation of feeding - bacteria from fecal pellets were cultured in kanamycin and ampicillin agar plates, demonstrating resistance of E. coli-mutant to kanamycin and E. coli-curli to ampicillin antibiotics, respectively. (E) There were equal copy numbers of the hSOD1 G93A transgene in mice in all 3 feeding groups. (F and G) There were no significant differences in body weights of mice from 1 to 7 months of age regardless of genotype and bacterial feeding. n=6-9 per cohort.

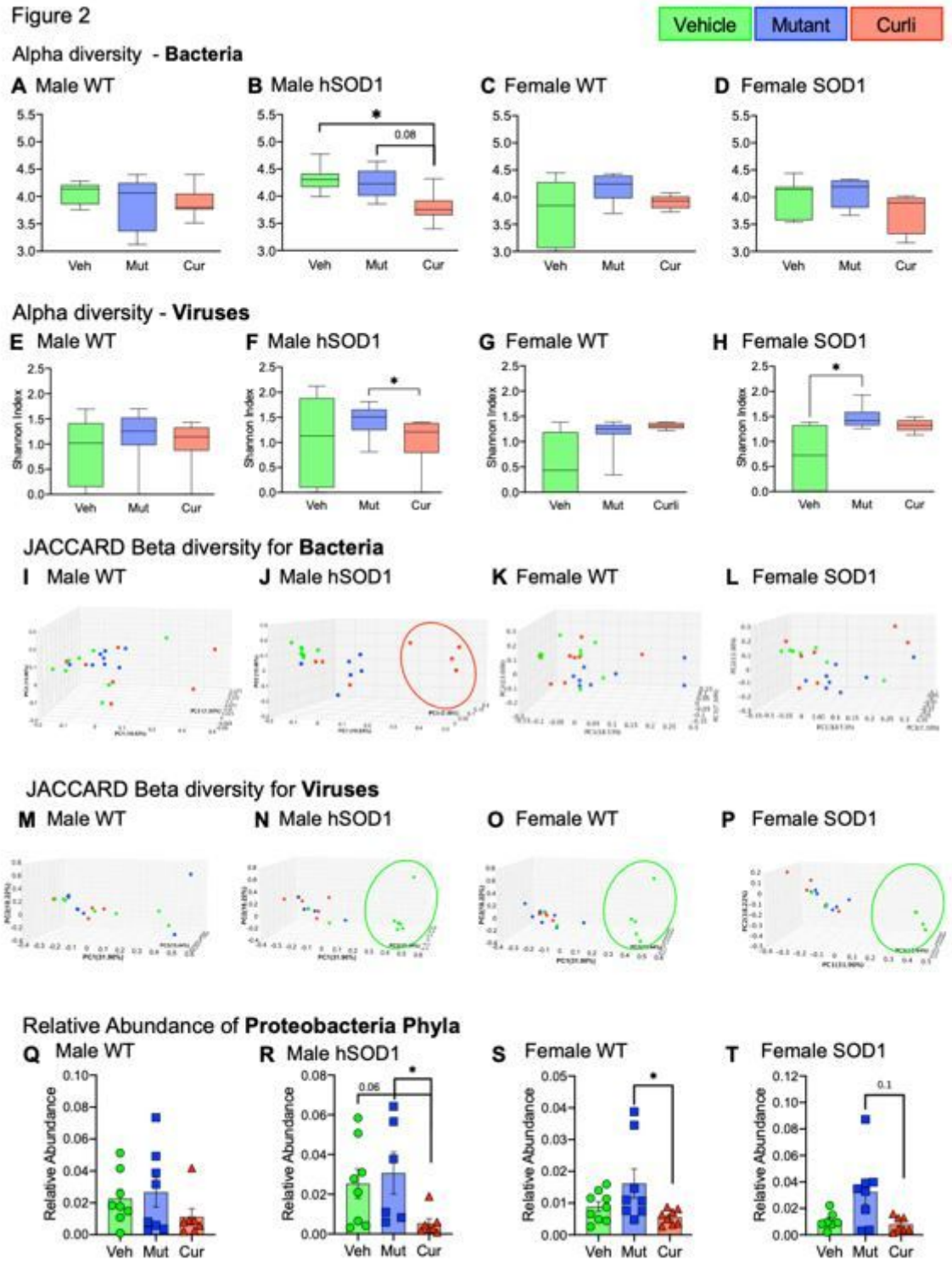

Figure 2

Whole-genome shallow shotgun sequencing analyses of fecal pellets at 6 months. (A-D) Within-group bacterial species diversity measured with Shannon alpha diversity index demonstrated poor species richness and abundance in curli-fed animals in the male hSOD1 cohort. *p<0.05, Wilcoxon Rank Sum test. (E-H) Within-group viral species diversity measured with Shannon alpha diversity index demonstrated poor species richness and abundance in curli-fed animals in the male hSOD1 cohort. *p<0.05, Wilcoxon Rank Sum test. (I-L) Between-group bacterial beta diversity measured with JACCARD index demonstrated distinct clustering of curli-fed animals in the male hSOD1 group. **p=0.001, PERMANOVA test. (M-P) Between-group viral species diversity measured by JACCARD index demonstrated distinct clustering of both bacterial-fed groups in male hSOD1, female WT and hSOD1 groups. **p<0.01, PERMANOVA test. (Q-T) Relative abundance of Proteobacteria phyla were significantly reduced in curli-fed male hSOD1 and female WT groups compared to mutant-fed groups. *p<0.01, Kruskal-Wallis test. n=6-9 per cohort.

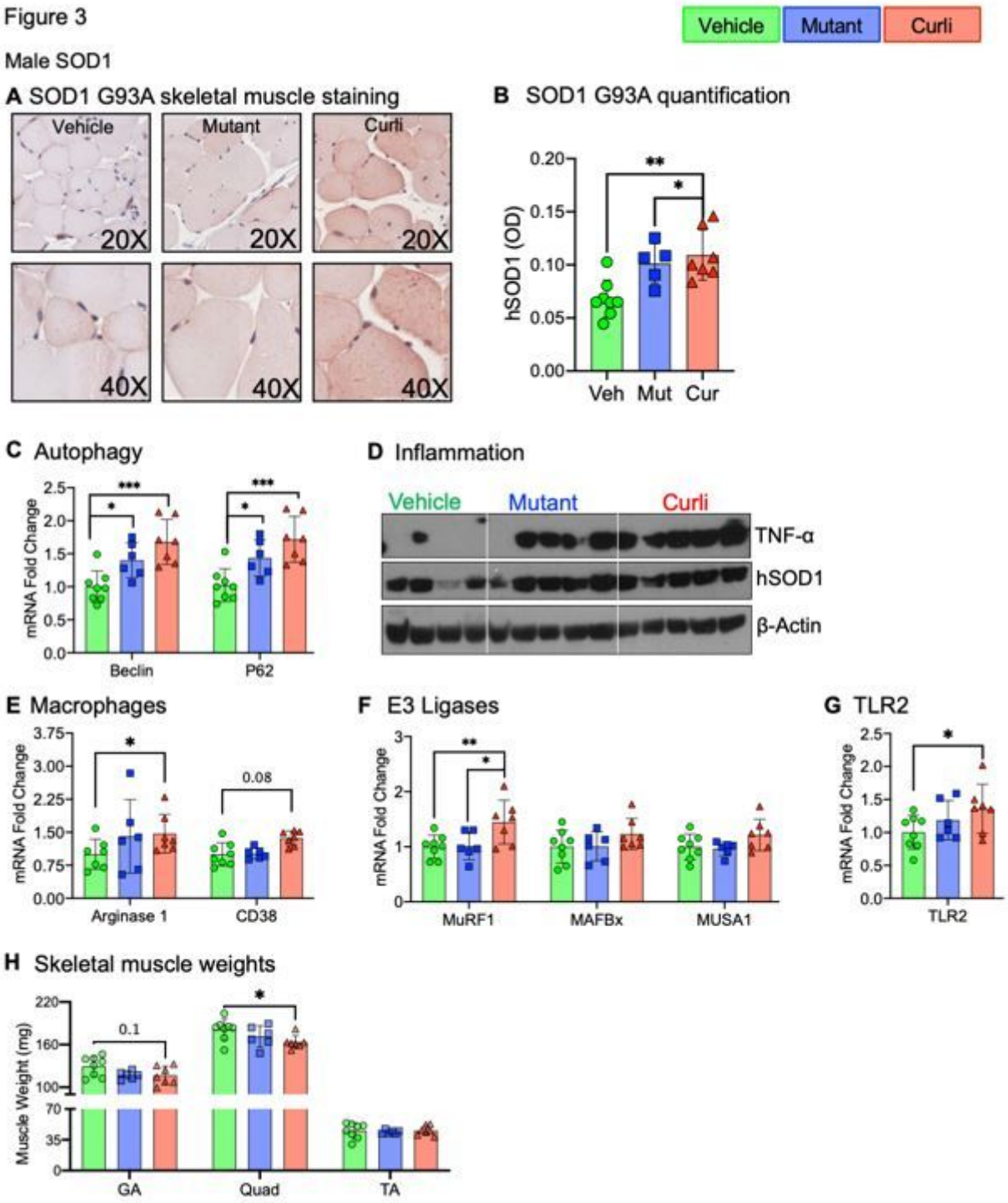

Figure 3

Markers of skeletal muscle atrophy by histochemical staining (tibialis anterior), Western Blot analysis (gastrocnemius) and qRT-PCR (gastrocnemius). (A, B) Mutant and curli-fed groups showed significantly increased immunostaining for hSOD1 in tibialis anterior muscles (C) qRT-PCR analysis demonstrated significantly increased expression of Beclin and p62 mRNA in curli-fed mice indicating increased autophagy in skeletal muscle (D) Western Blot analysis showed increased expression of pro-

inflammatory TNFα protein in mutant and curli-fed groups. (E) Inflammatory macrophage populations M1 (CD38) and M2 (Arginase 1), were both significantly elevated in gastrocnemius of curli-fed mice. (F) mRNA expression of an E3 ligase MurF1 was increased 1.5-fold in curli-fed male hSOD1 mice, indicating an increased turnover of myoproteins by the ubiquitin proteasome system. (G) mRNA expression of TLR2, a pathogen recognition receptor was significantly increased in gastrocnemius muscle in the curli-fed group. (H) Skeletal muscle weights of gastrocnemius (GA), quadriceps (Quad) and tibialis anterior (TA) were measured post-mortem and curli-fed mice had significantly lower weights of the quadriceps muscles compared to vehicle and mutant-fed groups. *p<0.01, **p<0.001, ***p<0.001 One or Two-way ANOVA. n=6-9 per cohort.

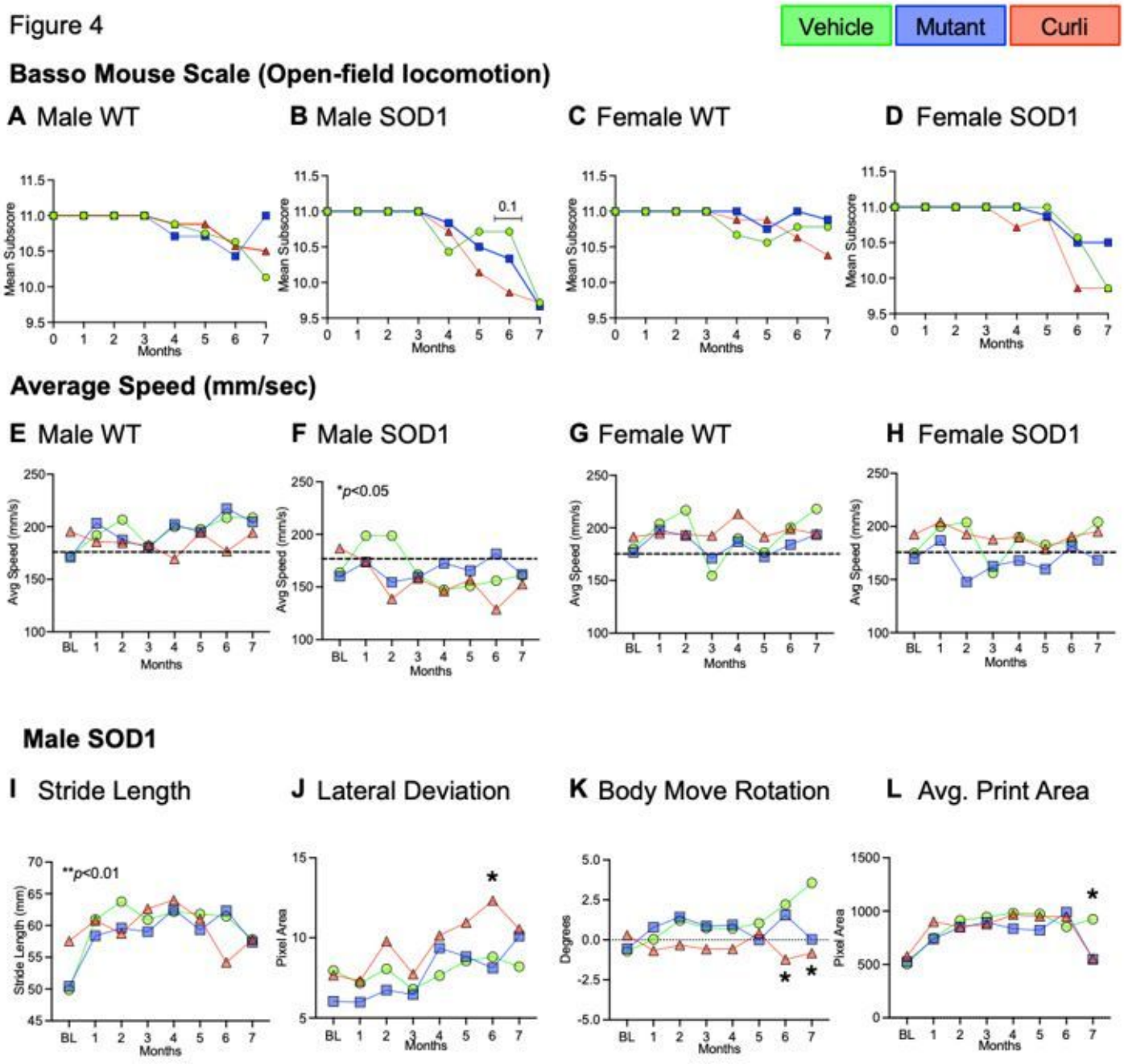

Figure 4

Locomotion characteristics (A-D) Open field locomotion of mice were evaluated using Basso Mouse Scale (BMS) from 3 weeks of age up to 7 months. BMS mean scores of mice in the hSOD1 groups (B, D) gradually declined compared to WT mice (A, C) as expected in ALS. Curli-fed male hSOD1 mice showed a trend ($p=0.1$) towards poorer BMS scores compared to vehicle group at month 6. (E-H) Average running speed measured with TreadScan software showed significant slowing of pace in male hSOD1 mice (F) compared to other cohorts (E, G, H). Within the male hSOD1 cohort, there was significant shortening in stride length (I) between the three feeding groups (**$p<0.01$), and curli-fed mice showed significant differences for maximum lateral deviation of hind feet from the axis of the body (J), inability to efficiently move body from a straight axis (K), and a smaller print area of the hind feet (L) towards later months. *$p<0.05$, Mixed-effects model analyses (REML) with Tukey's multiple comparisons. n=6-9 per cohort.

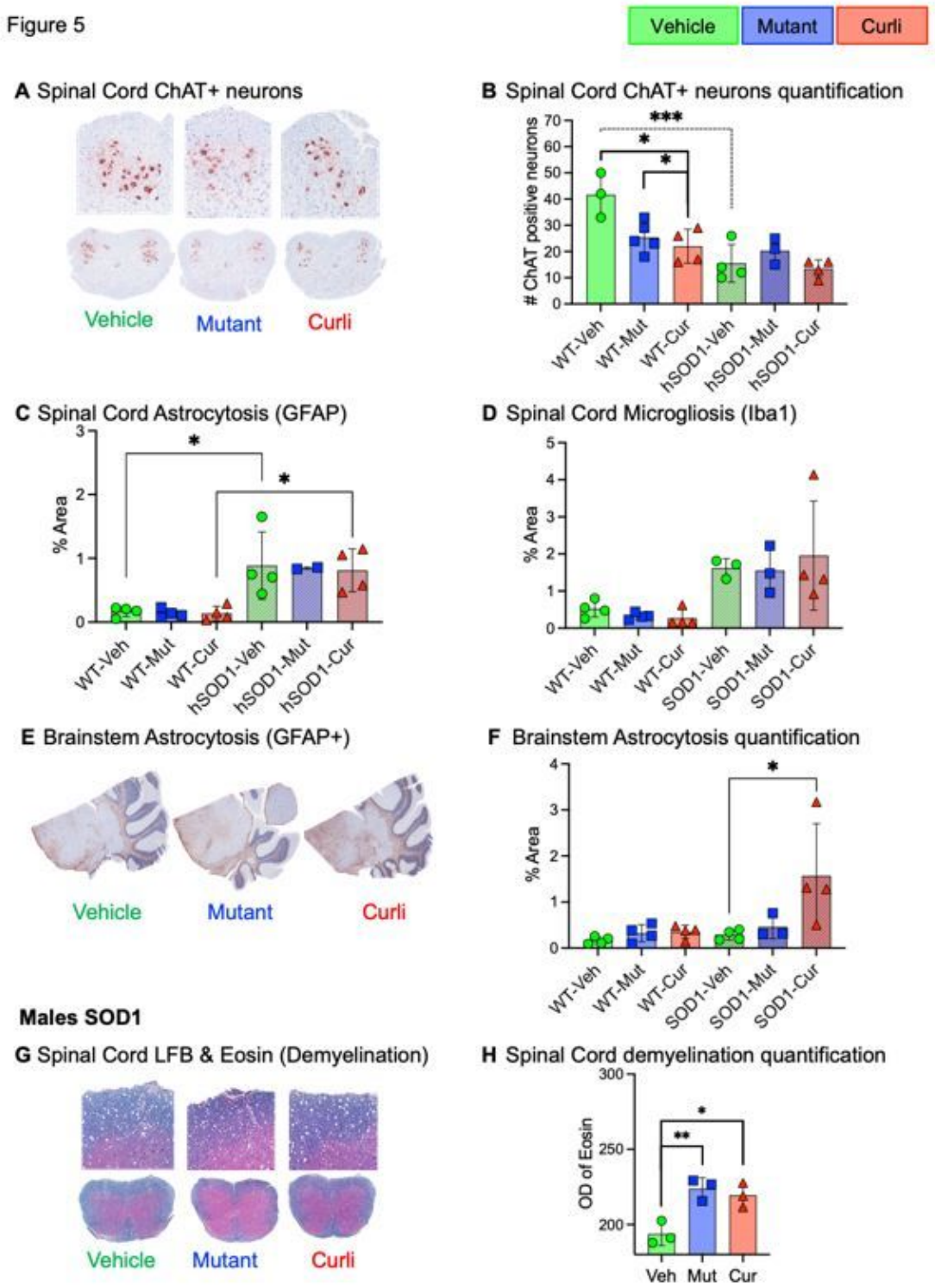

Figure 5

Alterations in the nervous system (A-C) In comparison to WT males, spinal cords of hSOD1 males had fewer ChAT positive neurons (B, ***p<0.001), increased astrocytosis (C) and microgliosis (D) but there were no significant differences between feeding groups within the hSOD1 cohort. However, within the male WT cohort, mutant and curli-fed mice had significantly decreased ChAT positive neurons (B, *p<0.05) compared to the vehicle group. Within the male hSOD1 cohort, curli-fed mice showed increased

staining of GFAP+ neurons (astrocytosis) in the brainstems (E, F) and mutant and curli-fed mice showed significant demyelination in white matter of spinal cords compared to vehicle groups (encroachment of pink cytoplasmic stain Eosin into areas of Luxol-Fast blue stained myelin). One-way ANOVA. n=2-5 per cohort.

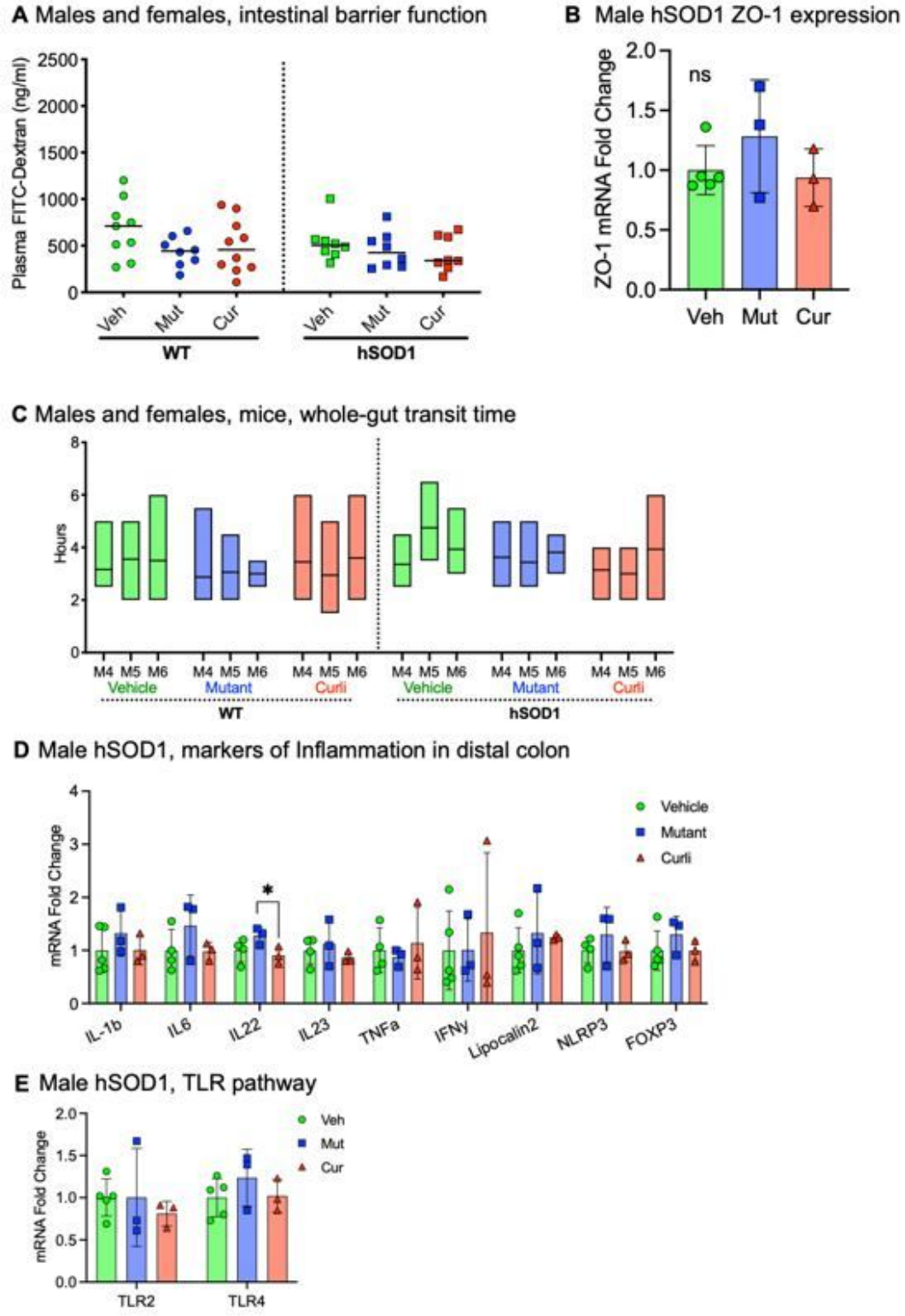

Figure 6

Functional characteristics of the gastrointestinal system (A) Gut barrier integrity was assessed by oral administration of FITC-Dextran and measuring its absorption into circulating blood 4 hours later. No significant breach in the gut barrier was detected in any mice. n=8-10, representative of both males and females. (B) Additionally, mRNA expression of ZO-1, a tight junction protein representative of an intact gut barrier was also not significantly altered between feeding groups in the male hSOD1 cohort. (C) There were no significant differences in whole-gut transit time between genotypes, sex or bacterial feeding groups measured as time taken (hours) to excrete carmine red dye administered orally. n=8-10, representative of both males and females. (D) Within the male hSOD1 cohort, there were no significant differences between bacterial groups for most markers of inflammation tested by qRT-PCR, except IL22 (trending, p=0.07, Kruskal-Wallis test). (E) mRNA expression of TLR2 and TLR4, known pathogen recognition receptors were not altered by bacterial feeding within the male hSOD1 cohort. n=3-5 per cohort.

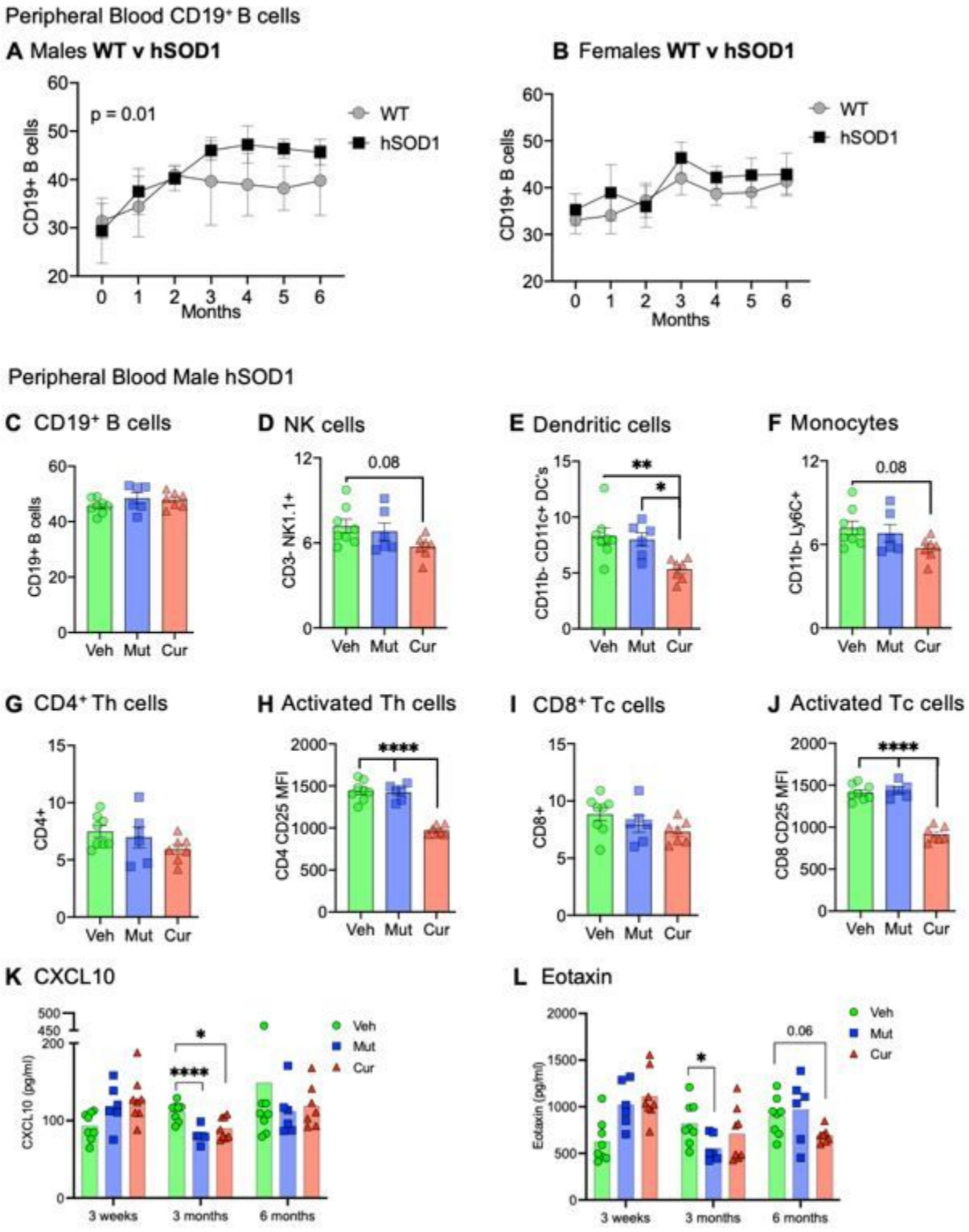

Figure 7

Peripheral blood immune responses (A) Immunophenotyping of peripheral blood demonstrated significantly increased CD19+ B cells in hSOD1 males compared to WT males, month 3 onwards. This phenomenon was not observed in female mice (B). (C-J) Within the male hSOD1 cohort, curli-fed mice exhibited significantly decreased markers of NK cells, dendritic cells, monocytes, activated TH cells and activated TC cells. (K, L) Pro-inflammatory cytokines CXCL10 (3 months) and eotaxin (6 months,

trending) were decreased in curli-fed male hSOD1 mice compared to vehicle groups. *p<0.01, **p<0.001, ****p<0.00001 Mixed-effects model analyses (REML). n=6-9 per cohort.